Optics Letters

Role of neutral impurities and non-parabolic dispersive electrons in HgCdTe avalanche photodiodes

Runzhang Xie,[1,†] Shuning Liu,[1,2,†] Xun Ge,[1,†] Haonan Ge,[1] Min Luo,[1] Anna Liu,[1] Qianlong Kang,[1] Chuan Shen,[1] Hao Xie,[1] Xiaohao Zhou,[1] Xiwen Liu,[2,3] Qing Li,[4] Lu Chen,[1,5] and Weida Hu[1,*]

[1]State Key Laboratory of Infrared Physics, Shanghai Institute of Technical Physics, Chinese Academy of Sciences, Shanghai 200083, China
[2]The Hong Kong University of Science and Technology (Guangzhou), Guangzhou 511453, China
[3]Electrical & Systems Engineering, University of Pennsylvania, Philadelphia, Pennsylvania 19104, USA
[4]Hangzhou Institute for Advanced Study, Hangzhou 310024, China
[5]Chenlu@mail.sitp.ac.cn
[†]These authors contributed equally to this work.
[*]wdhu@mail.sitp.ac.cn

Received 29 December 2024; revised 19 March 2025; accepted 20 March 2025; posted 20 March 2025; published 14 April 2025

HgCdTe avalanche photodiodes (APDs) exhibit unique gain stability, making them advantageous for weak signal detection. However, research on neutral impurities (NIs) scattering in HgCdTe remains limited, and the non-parabolic electron dynamics pose significant error in current device scale models. These limitations hinder the theoretical and the industrial development of HgCdTe APD. Here, we designed Si-substrate devices and CdZnTe-substrate devices with high and low NI density, respectively, to clarify the role of NIs. Combining first-principle calculations with Monte Carlo transport simulations, we find that the avalanching electrons could be categorized into four types (I–IV below) with distinct behavior. Furthermore, we proposed a step-solving Monte Carlo (SSMC) simulation framework to resolve accurately electron trajectories with non-parabolic dispersion. We then clarify different contemporary models of impact ionization and polar optical phonon scattering with SSMC and experimental results. Notably, our findings also show that Si-substrate HgCdTe APDs show nearly the same avalanche performance as the classical CdZnTe ones, suggesting that they could play a pivotal role in high-performance infrared detection in the future. © 2025 Optica Publishing Group. All rights, including for text and data mining (TDM), Artificial Intelligence (AI) training, and similar technologies, are reserved.

https://doi.org/10.1364/OL.554273

The mid-wave infrared (MWIR) from 3 to 5 μm has shown extensive application in various fields, particularly in thermal imaging, environmental monitoring, and defense technologies [1]. Currently, the area of infrared detection faces the bottleneck of weak radiation target detection and high circuit noise. In recent years, the emerging MWIR HgCdTe linear-mode avalanche photodiodes (APDs) have shown their unique advantage of low noise and high gain internal multiplication performance over traditional photovoltaic devices, their ultra-low noise and high gain make them promising for quantum key distribution (QKD) and LiDAR systems: under operating conditions, the linear APD has a definite gain (M) and a multiplied photocurrent (I). In signal processing, we assume M is a constant, and the target radiation flux Φ_e is derived with $\Phi_e \propto I/M$. Thus, any fluctuation of M in the denominator would introduce excess noise. This noise is characterized by the gain fluctuation [2,3] ($Gain\ Fluct. = \sigma(M)/M = \sqrt{\mathrm{ENF} - 1}$, where ENF is the excess noise factor). McIntyre's formula for *Gain Fluct.* is as follows:

$$Gain\ Fluct. = \sqrt{kM + (k-1)M^{-1} - 2k + 1}, \tag{1}$$

where k is the ratio of impact ionization coefficients for electrons (α) and holes (β). (β/α for electron APDs and α/β for hole APDs) [3] MWIR HgCdTe APD is typical electron APD.

In McIntyre's theory (Figs. 1(a) and 1(b)), *Gain Fluct.* cannot be less than 0.99 even when k approaches 0 at high gain ($M = 10^2$-10^3) condition. Despite McIntyre's theory has been validated in PIN APDs of Si, InGaAs, InP, etc. [4] As shown in Fig. 1(a), measured gain fluctuation of HgCdTe APDs from organizations SITP (≤0.305 [4]) and CEA/Leti (≤0.299 [5]) violate McIntyre's theory. The current explanation is primarily attributed to the history-dependent impact ionization process [6] and strong alloy scattering breaking the translational symmetry assumed in McIntyre's theory [7].

In APDs, electrons accelerate to high energy and undergo impact ionization. During this process, they are influenced by various scattering mechanisms. The influence of acoustic phonon scattering and inter-valley scattering has been proven to be negligible [7]. The influence of alloy scattering, ionized impurity scattering, impact ionization, polar optical phonon (POP) emission, and POP absorption has been proven to be significant and should be modeled carefully [5]. Among all scattering mechanisms in semiconductor physics, the last piece of

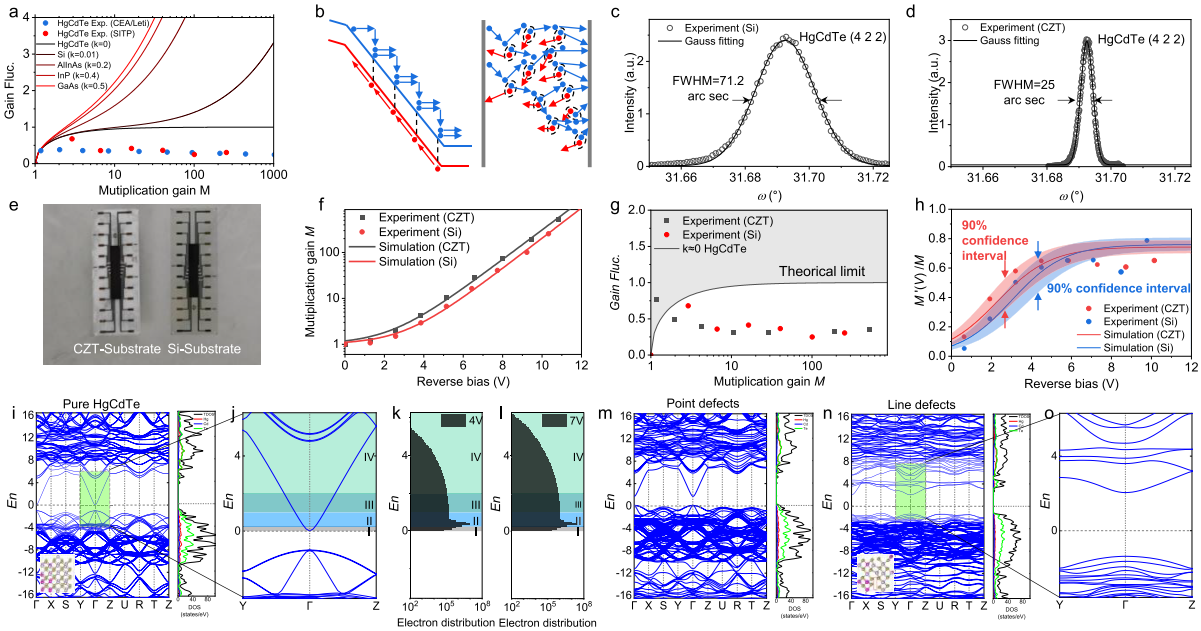


Fig. 1. Role of neutral impurities (NIs) in HgCdTe APDs. (a) Gain fluctuation derived from McIntyre's theory [4,5]. (b) Schematic of single-carrier avalanche. (c), (d) XRD result of Si- and CZT-substrate HgCdTe APD devices with the same crystal plane (4 2 2). (e) Images of fabricated CZT- and Si-substrate devices. (f) Measured (points) and fitted gain (curves), using Kinch's theory [7]) for Si- and CZT-substrate devices. (g) Measured gain fluctuation for Si- and CZT-substrate devices. (h) Relative change rate of gain, $M'(V)/M$ (using Kinch's theory). Shadow areas show the 90% confidence interval. (i) First-principle result of band structure and density of states (DOS) of pure HgCdTe. Inset: atomic structure of pure HgCdTe. (j) HgCdTe band structure avalanching electron can occupy. (k), (l) Transport Monte Carlo calculation of energy distribution of electrons in device at 4 V, and 7 V bias. (m)–(o) First-principle calculation of point defects and line defects in HgCdTe.

Table 1. Parameters of the Device Structure

Property	p-Region	i-Region	n^+-Region
Thickness (μm)	4.5 ± 0.5	4.5 ± 0.5	2
Doping density (cm^{-3})	$(7.8 \pm 1) \times 10^{15}$	$(2.5 \pm 0.5) \times 10^{14}$	6×10^{16}
Cd-component	0.33	0.33	0.33

the puzzle is neutral impurities (NIs) scattering. NI density is hard to be accurately measured. The bottleneck to clarify the scattering mechanisms is that there is no direct experimental evidence revealing the influence of NI-scattering, as well as its impact on M and *Gain Fluct.* To fabricate HgCdTe APDs with the same device parameters but drastically different NI density (Table 1, Fig. 1(e)). The difference in lattice mismatch between Si-substrate and CZT-substrate HgCdTe results in variations in NIs density. The x-ray diffraction (XRD) curves (Figs. 1(c) and 1(d)) reveal significant differences in lattice defects.

Photoelectric and noise characterizations of the Si- and CZT-substrate devices are performed by Kinch's theory (Supplement 1) and McIntyre's theory (Figs. 1(f) and 1(g)). The extracted gain threshold voltage of the Si- and CZT-substrate device is 3.03 V and 2.25 V, respectively. The low bias behavior is the result from the slightly different junction region introduced in the fabrication process. At high bias voltage, the gain's relative change ($M'(V)/M$) of Si- and CZT-substrate devices nearly completely overlap. The 90% confidence interval is shown as a reference (Fig. 1(h)). *Gain Fluct.* also shows similar behavior. They all indicate that the influence of the NI-scattering may be neglected in the HgCdTe avalanche process. However, in classical HgCdTe devices, the performance of Si-substrate devices differs significantly from that of CZT ones.

To clarify this anomaly, we combined first-principle calculations with transport Monte Carlo calculations to analyze the state the electron occupies in device, as shown in Figs. 1(i)–1(o). Figure 1 illustrates the energy band and density of states distribution for the HgCdTe device (Fig. 1(i)), point defects with Hg vacancies (Fig. 1(m)), and line defects in HgCdTe (Fig. 1(n)) (Supplement 1). Comparing transport Monte Carlo calculations with first-principle calculations, the electron states are categorized as quasi-equilibrium electrons near the band bottom (Type I), accelerated electrons with energy below the impact ionization threshold (Type II), electrons with energy above the impact ionization threshold but below the threshold for NI-scattering (Type III), and electrons with energy exceeding the threshold for NI-scattering (Type IV). First-principles calculations show Type I electrons slightly overlap with the valence band of point defects, as the behavior shown in classical HgCdTe devices. Type IV electrons overlap with the conduction band. For processes that influence the sensitive electron acceleration (Type II) process and energy regions just surpassing the impact ionization threshold (Type III), first-principle calculations indicate that the interaction between NI-scattering and electrons is negligible. At 4 V, the median energy for impact ionization-capable Type III and IV electrons corresponds to an electron impact ionization lifetime of $\tau_{ii} = P_{ii}^{-1}(E = 1.88E_g) = (1.91 \times 10^{10})^{-1} = 5.24 \times 10^{-11}$ s, where P_{ii} is the electron impact ionization rate [6]. If avalanche electrons are affected by NI-scattering, the threshold NI density would need to be on the order of $N_{ni}^{th} = (\tau_{ii} v_{sat} \sigma_{ni})^{-1} = 4.01 \times 10^{16}\,cm^{-3}$, where v_{sat} is the non-parabolic saturation velocity of HgCdTe conduction band

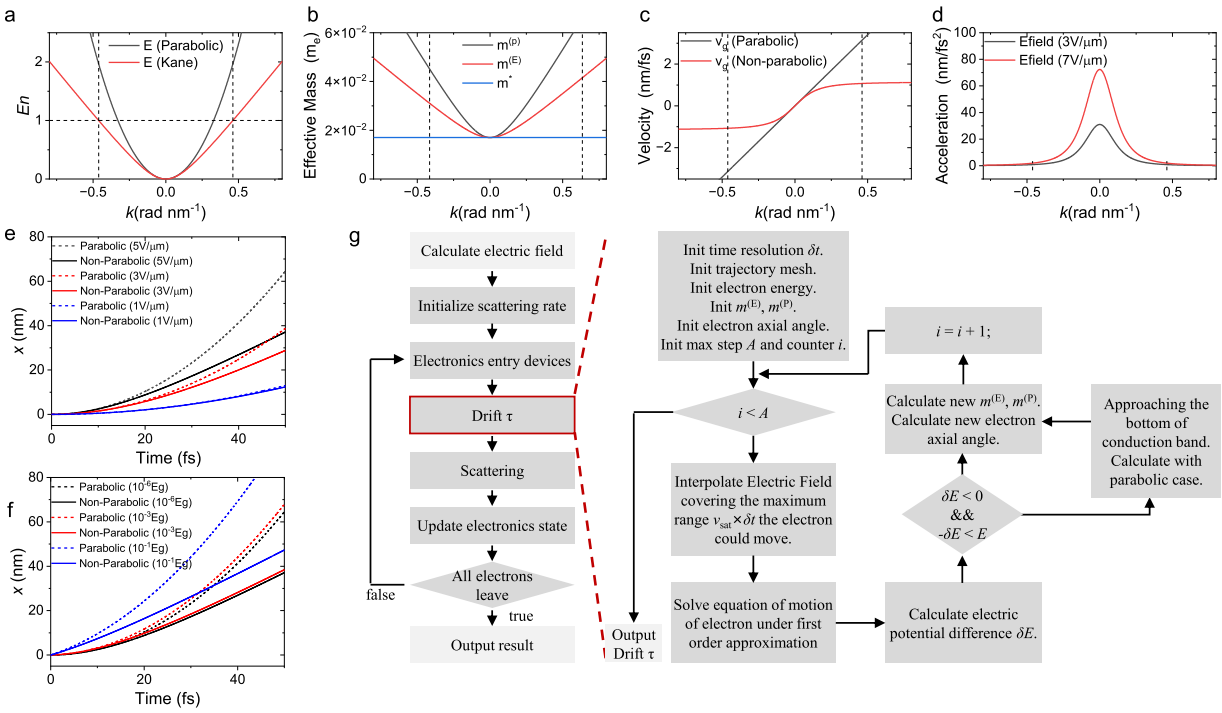


Fig. 2. Non-parabolic dispersive electrons in HgCdTe (Eg = 0.243 eV) APDs. (a) Parabolic and Kane non-parabolic conduction band. (b) Effective energy mass $m^{(E)}$ and effective momentum mass $m^{(P)}$. The horizontal line represents electronic mass m*. (c) Group velocity of electron in parabolic and non-parabolic. (d) Acceleration of electrons in different electric fields (3 V/μm and 7 V/μm). (e) Trajectory $x(t)$ of electron in 1 V/μm, 3 V/μm, and 5 V/μm electric fields in x direction. (f) Trajectory $x(t)$ of electron with initial velocity in yOz-plane and energy $10^{-6}Eg$, $10^{-3}Eg$, and $10^{-1}Eg$. (g) SSMC simulation framework for avalanche process of carriers with non-parabolic dispersion.

electrons [5] and σ_{ni} is the effective cross-sectional area for NI-scattering (assumed to be a_0^2 for an upper bound estimation of NI density; $a_0 = 6.47 \times 10^{-10}$ m is the HgCdTe lattice constant). At 7 V, $N_{ni}^{th} = 4.59 \times 10^{16}\,\mathrm{cm}^{-3}$. The total impurity concentration in Si-substrate HgCdTe is on the order of $10^{14}\,\mathrm{cm}^{-3}$, much lower than N_{ni}^{th}. According to first-principle calculations, only Class IV electrons interact with NI-scattering. The threshold density is $N_{ni}^{th} = 3.13 \times 10^{17}\,\mathrm{cm}^{-3}$ and $N_{ni}^{th} = 3.49 \times 10^{17}\,\mathrm{cm}^{-3}$ when the bias voltages are 4 V and 7 V, respectively. Thus, NIs primarily influence dark current via Type I, while Type II and III electrons affect the avalanche. Although NIs also impact the avalanche through Type IV, the fraction of electrons in Type IV interacting with NIs is negligible.

With previous works by Kinch *et al.* [7], Derelle *et al.* [5], and Bertazzi *et al.* [8], we develop a Monte Carlo framework for HgCdTe avalanche process without any fitting parameter. For electron drift process in the device, in Kane's theory [7] $E = \frac{E_g}{2}\sqrt{1 + 2\hbar^2k^2/E_g m_o^*} - \frac{E_g}{2}$, where the non-parabolicity factor $\alpha_c = 1/E_g(1 - m_c^*/m_0)^2$ depends on the bandgap. In narrow bandgap materials like HgCdTe and InAsSb, non-parabolicity significantly affects the electron dynamics. As the electron energy increases (Figs. 2(a)–2(d)), the effective momentum mass $m^{(P)}$ and the effective energy mass $m^{(E)}$ [6] continue to increase, while the group velocity tends v_{sat}. Importantly, the acceleration gradually decreases to 0 (Fig. 2(d)) when the group velocity tends v_{sat}, weakening the pulling effect of the electric field (Fig. 2(e)), especially when the electron has a high velocity perpendicular to the direction of electric field (Fig. 2(f)).

To obtain the trajectory of an electron in a non-parabolic band, the nonlinear motion equation coupled with electron's direction of motion as follows:

$$\begin{cases} f = eE_x m^{(E)}/m^{(P)} \\ p^2 = 2m^{(E)}E \\ p_x = \sqrt{p^2 - p_{yz}^2} \\ m^{(E)} = m_c^*(1 + \alpha_c E) \\ m^{(P)} = m_c^*(1 + 2\alpha_c E), \end{cases} \tag{2}$$

needs to be solved, where f is the force exerted on an electron in a non-parabolic band, e is the charge of the electron, E_x is the electric field in the x direction, p is the momentum of the electron, α_c is the non-parabolicity factor, and p_x and p_{yz} are the momentum of the electron in the x direction and yOz-plane, respectively. E is the energy of the electron. During the Monte Carlo calculations, directly solving the equations is computationally expensive even for a supercomputer, which hinders this technical pathway. By introducing pre-solving and piecewise solving methods (Fig. 2(g)), we developed a step-solving Monte Carlo (SSMC) simulation framework that can be performed within an acceptable resource consumption. The Monte Carlo algorithm incorporates all scattering models based on Fermi's golden rule (alloy scattering, impact ionization, POP scattering, etc.), implemented without any fitting parameter using C++ and MPI on *Sugon* supercomputer. Specifically, the POP scattering rate in non-parabolic band is derived from Fermi's golden rule based on previous work for the parabolic band. By considering the momentum and energy conservation in a non-parabolic band, we find that the modified scattering formula for POP from the parabolic case to the non-parabolic requires only a transformation (Supplement 1) $\omega_\beta \rightarrow \omega_\beta\sqrt{2\alpha_c p^2/m_c^* + 1}$ on the POP scattering rate, where α_c is the non-parabolicity factor, ω_β is the frequency of the POP mode, and m_c^* represents the effective mass in the conduction band.

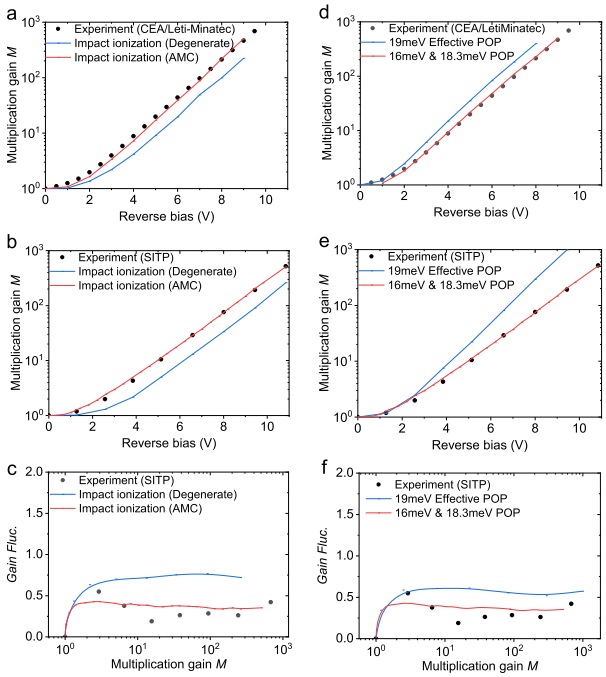


Fig. 3. Step-solving Monte Carlo of HgCdTe APDs. Simulation and experimental results with (a)–(c) different impact ionization models and (d)–(f) different POP models. Experimental result in (a) and (d) are based on CEA/Leti's report [5]. Experimental result in (b), (c), (e), and (f) are of device shown in Fig. 1(d), measured in SITP.

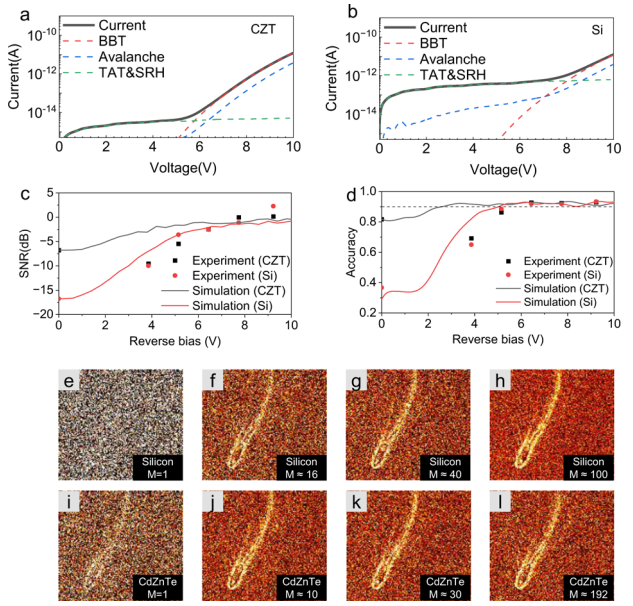


Fig. 4. Performance comparison between Si- and CZT-substrate HgCdTe APDs. (a), (b) Dark current analysis of device on CZT- and Si-substrate (including BBT, Avalanche, and TAT&SRH). (c) Device SNR on CZT- and Si-substrate. (d) Recognition accuracy for Si- and CZT-substrate devices. Calculation is performed according to the measured gain and its fluctuation in Figs. 1(e)–1(l). Simulation of imaging quality of Si- and CZT-substrate HgCdTe APD devices under different gain conditions.

Two widely used models for impact ionization are the degenerate valence band density of states [7] and the model that conserves angular momentum during the scattering (AMC) [6]. Two widely used models for POP scattering, models based on a 19 meV equivalent POP mode and two non-parabolic POP modes at 16 meV and 18.3 meV [8], have been proposed. With SSMC simulation framework based on Fermi's golden rule and non-parabolic dynamics, we find that the combination of impact ionization model with angular momentum-conservation and POP model considering at 16 meV and 18.3 meV with non-parabolic electron dispersion is closer to the experimental results (Fig. 3).

Focusing on the demand for high-performance infrared focal plane arrays in industry , large-diameter heteroepitaxial devices on Si substrates are being employed, significantly reducing material costs and driving the development of Si-substrate HgCdTe devices. However, these devices encounter challenges of dark current and noise-blind pixels led by NIs. Under avalanche conditions, we find NI-scattering in Si-substrate devices is weak, resulting in similar photoelectric current gain and noise performance compared to CZT-substrate devices. We also find the dark current components in CZT-substrate and Si-substrate devices are driven by TAT (trap-assisted tunneling), BBT (band-to-band tunneling), or impact ionization (Figs. 4(a) and 4(b)), in contrast to the dark current dominated by the SRH (Shockley–Read–Hall) mechanism related to NIs under low bias voltage (Supplement 1). This led to a similar signal-to-noise ratio (SNR) for both Si-substrate and CZT-substrate HgCdTe APD devices (Fig. 4(c)). Even in target recognition applications (Fig. 4(d)) and imaging simulations of both CZT-substrate and Si-substrate devices (Figs. 4(e)–4(l)), under high gain and high bias, the imaging quality of Si-substrate devices gradually approaches that of CZT-substrate devices, which shows an important developmental direction for MWIR detection.

Funding. Strategic Priority Research Program (B) of the Chinese Academy of Sciences (XDB0580000, XDB0980000); National Natural Science Foundation of China (62205360).

Disclosures. The authors declare no conflicts of interest.

Data availability. Data underlying the results presented in this paper are not publicly available at this time but may be obtained from the authors upon reasonable request.

Supplemental document. See Supplement 1 for supporting content.

REFERENCES

1. C. Rogers, A. Y. Piggott, D. J. Thomson, *et al.*, Nature **590**, 256 (2021).
2. P. Martyniuk, P. Wang, A. Rogalski, *et al.*, Light: Sci. Appl. **12**, 212 (2023).
3. R. J. McIntyre, IEEE Trans. Electron. Devices **ED-13**, 164 (1966).
4. L. Zhu, H. Ge, H. Guo, *et al.*, IEEE Trans. Electron. Devices **70**, 2384 (2023).
5. S. Derelle, S. Bernhardt, R. Hardar, *et al.*, IEEE Trans. Electron. Devices **56**, 569 (2009).
6. R. Xie, Q. Li, P. Wang, *et al.*, Opt. Express **29**, 16432 (2021).
7. M. A. Kinch, J. D. Beck, C.-F. Wan, *et al.*, J. Electron. Mater. **33**, 630 (2004).
8. F. Bertazzi, M. Moresco, M. Penna, *et al.*, J. Electron. Mater. **39**, 912 (2010).